Analytical Solution of Forced Convective Heat Transfer in a Horizontal Anisotropic Porous Media Cylinder: Effect of Variations of Frictional Heating and Heat Generation on the Temperature Profile and Nusselt Number

H. Soltani[a,*] and H. Ajamein[b]

[a]Department of Chemical Engineering, Ahar Branch, Islamic Azad University, Ahar, Iran

[b]Department of Chemical Engineering, Ilkhchi Branch, Islamic Azad University, Ilkhchi, Iran

doi: 10.15255/CABEQ.2014.2013

Original scientific paper
Received: March, 9, 2014
Accepted: September 6, 2014

This paper presents the study of the effects of anisotropy on fully developed forced convection heat transfer in a horizontal cylinder with a constant heat flux applied on its outer wall side. By applying mathematical model, using continuity, momentum and energy equations, the effects of essential parameters, such as A^*, Darcy number *Da*, modified Brinkman number Br^*, as well as the presence or absence of heat generation and fractional heating on the heat transfer and fluid flow characteristics, in the horizontal cylinder were determined and depicted in graphs. Consequently, it was found that for a particular value of A^* (called A^*_c), the sign of Nusselt number changed. Also, for special values of A^* (called A^*_V), the relative Nusselt number deviations δ which show the relative deviations between Nusselt number with and without frictional heating term, do not change with *Da* numbers.

Key words:

forced convection, horizontal cylinder, anisotropic porous media, heat generation, frictional heating, Nusselt number deviations

Introduction

Anisotropy is the result of optional orientation or geometric asymmetry caused by the position of particles in an object. This property of material influences convection heat transfer of objects two ways: hydrodynamic permeability and thermal diffusion due to changes of thermal conductivity.[1] There are various applications for the effect of anisotropy on heat transfer, such as: nuclear industries,[2] geology,[3] water resource management,[4,5] oil and gas,[6] and fixed bed reactors.[7] Porous beds are one of the very applicable research areas of the field of heat transfer based on anisotropy. Research on the effect of anisotropy on heat transfer can be categorized based on heat transfer regimes, the variety of materials and the applied solution methodology.[8] In terms of the type of heat transfer regimes, natural convection,[9–11] forced convection,[12–14] and mixed convection[15,16] have been studied, where natural convection is more noticeable. Horizontal, vertical and inclined rectangular or cylindrical objects were studied to investigate the effect of anisotropy on convection heat transfer. The governing equations were solved by numerical or analytical methodologies.[17]

In early studies of convection heat transfer in porous beds, the term of anisotropy had been ignored. The first studies examining the effects of anisotropy were performed by Castinel and Combarnous on free convection over a horizontal plane with anisotropic permeability.[18] The anisotropic thermal diffusion was investigated by Epherre, who determined that anisotropy effects on the thermal properties influence the marginal stability criterion as the preferred width of the convection cells.[19] Their studies were completed by Kvernold and Tyvand to analyze the effects of anisotropy in permeability on the critical Rayleigh number for the onset of convection and attitude of convective flow at slightly supercritical Rayleigh numbers.[20] Tyvand and Storesletten studied natural convection in an anisotropic medium where none of the principal axes were vertical by considering Benard convection in a horizontal porous layer with anisotropic permeability.[21]

Recently, some research has been directed to the effect of anisotropy on the onset of convection

* Corresponding author: email: h-soltani@iau-ahar.ac.ir, tel.:+98 426 2232176, fax: +98 426 2227872

in porous layer.[22,23] The mixed convection through a parallel-plate vertical porous channel, which was assumed to be hydrodynamically anisotropic, was studied by Degan and Vasseur.[16] They found that for $Da < 10^{-5}$ the viscous effects near the boundaries were negligible, and the permeability ratio and inclination of principal axes of permeability had a strong influence on the thermal convection. The effect of gross heterogeneity in forced convection in a porous media filled channel was studied by Kuznestsov and Nield.[24] They estimated the Nusselt number and discovered that an increase in Nu/f (f is the friction factor) resulted with an increase in heat transfer. The mechanism of heat and fluid flow in a channel with internal heat generation due to viscous dissipation for constant heat flux boundary conditions in a parallel-plate horizontal channel filled with an anisotropic permeability porous medium was analytically deliberated by Mobedi *et al.*[12] They proved that the directional permeability parameter, which was defined to combine the effect of permeability ratio and the orientation angle, had an important effect on the mechanism of heat and fluid flow in the channel. Hence, by increasing the directional permeability parameter, high velocity gradient appeared in the region close to the channel wall and caused high internal heat generation in regions close to the walls.

The forced convection heat transfer in two channel configurations (parallel plates and a circular pipe) were investigated by Poulikakos and Renken. These two channels were assumed to fill with porous media. By assuming constant thermal conductivity, they achieved a model by governing equations based on the effects of flow inertia, variable porosity and Brinkman friction, and finally solved it by a numerical method. Consequently, they found that the velocity field resulting from the solution of general momentum equation significantly changed the heat transfer characteristics compared to the systems using Darcy flow model.[25]

The fully developed laminar steady forced convection inside a circular tube filled with saturated porous medium with uniform heat flux at the wall was studied by Hooman and Ranjbar-Kani. They described that the velocity profile depended strongly on s parameter ($S = (1/(M \cdot Da))^{1/2}$, where M is viscosity ratio, and Da is the Darcy number). When s increases, the central region containing a uniform velocity distributes toward the wall, while if it decreases, the velocity tends toward the plane Poiseuille flow. In addition, the Nusselt number depends on s magnitude and increases with its enhancement.[26]

In contrast to many investigations that considered the anisotropy effects on convection heat transfer in Cartesian coordinates, few researches have paid attention to its effects in cylindrical coordinates. Minkowycz and Cheng studied the natural convection heat transfer around a vertical cylinder immersed in porous media while its surface temperature changed as a power function over the edge.[27] Vasantha and Nath investigated the thermal boundary layer around an isotherm cylinder in porous media numerically, and found that the thickness of the thermal boundary layer increased with enhancement of the transverse curvature parameter.[13] Degan *et al.* investigated the effect of the anisotropic hydrodynamic permeability parameter on convection heat transfer in a vertical cylinder filled with porous media. They understood that both the anisotropic hydrodynamic permeability parameter, and the orientation angle of the principal axes had a significant influence on the heat transfer rate.[28] The effect of anisotropy on hydrodynamic permeability and thermal diffusion of natural heat convection in a vertical cylinder filled with porous media and a heat generation source, was studied by Dhanasekaran *et al.* They demonstrated that both the hydrodynamic permeability ratio and the thermal diffusion ratio caused enhancement of heat transfer rate separately.[10]

This paper presents an analytical study of steady force convection heat transfer inside an anisotropic porous cylinder with oblique principal axes, using the extended Darcy-Brinkman model with the aim of investigating the effects of anisotropic permeability. In addition, the effects of the presence or absence of frictional heating term, the heat generation in the porous channel on the temperature profile, and Nusselt number were studied.

This kind of problem is common with horizontal cylindrical fixed bed catalytic reactors in which exothermic reactions occur. In fixed bed catalytic reactors filled with anisotropic porous media named heterogeneous catalysts, forced convection heat transfer occurs inside the reactor by gas stream movement. On the other hand, an exothermic reaction can create a heat generation source inside the reactor, which rises the temperature of the reactor and may cause hot spots on the catalysts, and finally deactivate the catalyst. Therefore, cooling heat flux is applied on the outside walls of the reactors to control this heat generation. Anisotropic properties of filled catalysts in the reactor face us with an anisotropic forced heat convection. Thus, temperature control and optimized heat transfer in these reactors, which are applied in many petrochemical and refinery units, seem quite important. Therefore, investigation of the parameters having a significant effect on velocity and temperature profiles, and the Nusselt number, could suggest applicable solutions

for better temperature control of these reactors and thus acquire high yield for products, and increase the useful life of catalysts.

Therefore, this paper is organized in the following manner: The model, and the governing equations and their solutions are presented in the next section, while the following section describes and discusses briefly the results of the problem, and last section is the conclusion of the paper.

The model and the governing equations and solutions

Model description and governing equations

The geometry and boundary conditions of two-dimensional horizontal cylinder containing porous media, which is considered in this work, are schematically shown Fig. 1. The radius of the cylinder is R and fluid flows in the direction of z-axis, perpendicular to radial direction (r). For simplification, the radial angle is ignored.

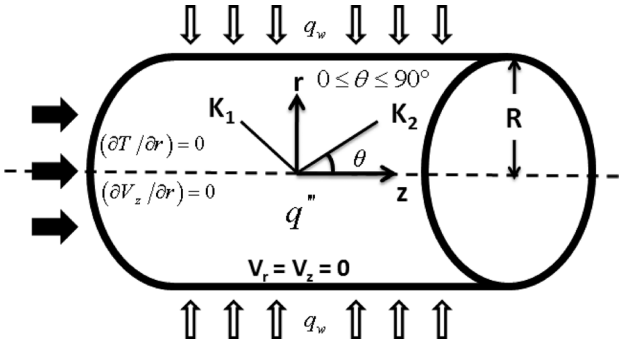

Fig. 1 – *Physical model and coordinate system*

The porous media in the cylinder are anisotropic in permeability properties. Permeability parameters along the two principal axes of the porous matrix are denoted by K_1 and K_2 respectively.

As depicted in Fig. 1, the anisotropy of the porous medium is characterized by the orientation angle θ and the permeability ratio parameter $K^* = K_1/K_2$. Other assumptions for this model are as follows: fluid flow is one-dimensional and fully developed, steady state conditions, no phase changes, constant heat flux is applied to horizontal walls, and uniform heat generation exists in the cylinder.

Therefore, by mentioning problem conditions the governing equations for a laminar flow passing through this cylinder are continuity, Brinkman momentum, and energy, which are represented as follows:

$$\nabla\vec{V} = 0 \Rightarrow \frac{1}{r}\frac{\partial}{\partial r}\left(rV_r\right) + \frac{\partial V_z}{\partial z} = 0 \tag{1}$$

$$\vec{V} = \frac{\overline{\overline{K}}}{\mu}\left(-\nabla p + \tilde{\mu}\nabla^2\vec{V}\right) \tag{2}$$

$$\rho C_P \nabla(T\vec{V}) = \nabla(k\nabla T) + \left[C_1\frac{\mu}{K_1}V_z{}^2 + C_2\tilde{\mu}\left(\frac{\partial V_z}{\partial y}\right)^2\right] + C_3 q''' \tag{3}$$

The symmetrical second order permeability tensor $\overline{\overline{K}}$ is defined as follows:

$$\overline{\overline{K}} = \begin{bmatrix} a & b \\ b & c \end{bmatrix}$$

$$a = K_2\cos^2\theta + K_1\sin^2\theta \tag{4}$$

$$b = \left(K_1 - K_2\right)\sin\theta\cos\theta$$

$$c = K_2\sin^2\theta + K_1\cos^2\theta$$

In the above equations (Eqs. (1–4)) $\vec{V}$ is the superficial flow velocity vector, V_r is the velocity in r-direction, V_z is the velocity in z-direction, p is the pressure, T is the volume-averaged equilibrium temperature for both the solid and fluid phases of the porous medium, ρ is the fluid density, μ is the fluid viscosity, $\tilde{\mu}$ is the effective viscosity for Brinkman's model, C_p is the specific heat at constant pressure, K_1 and K_2 are the flow permeabilities along the principle axes, q''' is the heat generation, and C_1, C_2 and C_3 are constant values (their values can be 0 or 1), which describes the presence or absence of viscous dissipation and heat generation parameters. The viscous dissipation effect considered on the right hand side of energy equation is composed of two parts. The first part, namely $\left(\mu/K_1\right)V_z{}^2$, is the viscous dissipation in the Darcy limit ($K_1 \to 0$), which basically comprises the internal heating associated with the mechanical power needed to extrude the fluid through the porous medium as given by Ingham *et al.*,[29] while the second part, namely $\tilde{\mu}\left(\partial V_z/\partial y\right)^2$, is the frictional heating term involving fluid friction due to dissipation, as given by Al-Hadhrami *et al*.[15]

Solution of Brinkman momentum equation

According to assumptions for 2-D fully developed fluid flow considered to be laminar flow, it can be assumed that the following expressions are acceptable.

$$V_r = 0, \quad \frac{\partial V_z}{\partial z} = 0, \quad \frac{\partial p}{\partial r} = 0 \tag{5}$$

So, the Brinkman moment equation (Eq. (2)) can be simplified as follows:

$$r\frac{d}{dr}\left(r\frac{dV_z}{dr}\right) - \left(\frac{A^*}{K_1 M}\right)r^2 V_z = -\left(\frac{\gamma}{M}\right)r^2 \tag{6}$$

By following boundary conditions:

$$V_z(r=R)=0, \qquad \left(\frac{dV_z}{dr}\right)_{r=0}=0 \tag{7}$$

Where

$$A^*=\sin^2\theta+K^*\cos^2\theta, \quad K=K_1/K_2,$$
$$\gamma=-\frac{\partial}{\mu\,\partial}, \qquad =\mu/\mu \tag{8}$$

In these equations, M and γ are the dimensionless viscosity parameter and negatic of the applied pressure gradient, respectively, defined by Hung and Tso,[30] and A^* is the directional permeability ratio parameter.

The boundary conditions in differential equation (Eq. (7)) are defined by employing a no-slip wall boundary condition and symmetry condition at the centre of the cylinder. By introducing dimensionless parameters such as anisotropic shape factor α, Darcy number Da, and dimensionless coordinate in r direction r^* as follows:

$$\alpha=\sqrt{\frac{A^*}{MDa}}, \quad Da=\frac{K_1}{R^2}, \quad r^*=\frac{r}{R} \tag{9}$$

Eq. (6) and its boundary conditions are changed to:

$$r^*\frac{d}{dr^*}\left(r^*\frac{dV_z}{dr^*}\right)-\alpha\left(r^*\right)^2V_z=-\left(\frac{\gamma R^2}{M}\right)\left(r^*\right)^2 \tag{10}$$

$$V_z\left(r^*=1\right)=0, \qquad \left(\frac{dV_z}{dr^*}\right)_{r^*=0}=0 \tag{11}$$

This is a second order inhomogeneous differential equation.

The analytical solution of Eq. (10) with respect to its boundary conditions Eq. (11) can be found as follows:

$$V_z(r^*)=\frac{\gamma K_1}{A^*}\left[1-\frac{I_0\left(\alpha r^*\right)}{I_0(\alpha)}\right] \tag{12}$$

Considering Eq. (12), the average velocity $\overline{V_z}$ and the normalized dimensionless velocity $V^*(r^*)$ can be defined as follows:

$$\overline{V_z}=\left(\int_0^1 r^*V_z dr^*\right)\Big/\left(\int_0^1 r^*dr^*\right)=\frac{R^2\gamma}{M\alpha^2}\left[1-\frac{2I_1(\alpha)}{\alpha I_0(\alpha)}\right] \tag{13}$$

$$V^*(r^*)=\frac{V_z(r^*)}{\overline{V}_z}=\frac{\alpha\left[I_0(\alpha)-I_0\left(\alpha r^*\right)\right]}{\left[\alpha I_0(\alpha)-2I_1(\alpha)\right]} \tag{14}$$

Solution for heat transfer equation

By applying the assumptions for the model in the porous medium, and considering that the Peclet number is sufficiently large so the axial conduction may be neglected, the heat transfer equation (Eq. (3)) can be simplified into the following form.

$$\rho c_p V_z\frac{\partial T}{\partial z}=k\left(\frac{1}{r}\frac{\partial}{\partial r}\left(r\frac{\partial T}{\partial r}\right)\right)+ \\ +C_1\frac{\mu}{K_1}V_z{}^2+C_2\tilde{\mu}\left(\frac{dV_z}{dr}\right)^2+C_3q''' \tag{15}$$

With the following boundary conditions:

$$\left(\frac{\partial T}{\partial r}\right)_{r=0}=0, \quad \left(\frac{\partial T}{\partial r}\right)_{r=R}=\frac{q_w}{k} \tag{16}$$

Where q_w is negative and q''' is positive for cooling process (fluid being cooled). The first boundary condition comes from the symmetry condition at the centre of the channel and the second is defined from the constant wall heat flux boundary condition.

Integral method was applied to find analytical solutions for the temperature equation. First, the sides of Eq. (15) were multiplied by r and then integrated from centre of the cylinder to the diameter of the cylinder R.

$$\rho c_p\frac{\partial}{\partial z}\int_0^R rV_zT\,dr=Rq_w+C_1\int_0^R\frac{\mu}{K_1}rV_z{}^2\,dr+ \\ +C_2\int_0^R r\tilde{\mu}\left(\frac{dV_z}{dr}\right)^2dr+C_3\int_0^R q'''rdr \tag{17}$$

For the left side of Eq. (17) from definition of the average temperature, it would be:

$$\int_0^R rV_zT\,dr=\frac{\int_0^R rV_zTdr}{\int_0^R rV_z\,dr}\int_0^R rV_z\,dr= \\ =\overline{T}\frac{\int_0^R rV_z\,dr}{\int_0^R rdr}\int_0^R rdr=\overline{T}\overline{V_z}\frac{2}{R^2} \tag{18}$$

For thermally fully developed flow, the temperature gradient along the axial direction z is independent of the transverse direction r, Hung and Tso,[30] therefore, $\partial T/\partial z=d\overline{T}/dz$. According to boundary conditions defined in Eq. (16), the Eq. (17) can be applied as follows:

$$\rho C_P\frac{d\overline{T}}{dz}=\frac{q_w}{R\overline{V_z}}\left(2+\frac{Br^*\alpha^2}{\eta^2Da}\left(C_1\left[2-\lambda^2-\frac{4}{\alpha}\lambda\right]+\right.\right. \\ \left.\left.+C_2MDa\left[\lambda^2+\frac{2}{\alpha}\lambda-1\right]\right)+C_3\beta\right) \\ Br^*=\frac{\mu\overline{V_z}^2}{Rq_w}, \ \beta=\frac{Rq'''}{q_w}, \\ \eta=\left[\left(1-\frac{2}{\alpha}\lambda\right)^2\right]^{-1}, \ \lambda=\left(\frac{I_1(\alpha)}{I_0(\alpha)}\right) \tag{19}$$

where $\overline{T}$ is the average temperature along sectional area of cylinder, Br^* dimensionless modified Brinkman number, β dimensionless term of heat flux and heat generation, η and λ dimensionless parameters which are a function of anisotropic shape factor α. By introducing the following dimensionless temperature function $T^*(r^*)$ as:

$$T^*\left(r^*\right) \quad \frac{k\left(T \quad T\right)}{Rq}, \tag{20}$$

Eq. (15) can be written as:

$$\frac{d}{dr^*}\left(r^*\frac{dT^*}{dr^*}\right)=\left[2+C_1\frac{\psi(\alpha)}{Da}Br^*+\right.$$
$$\left.+C_2M\phi(\alpha)Br^*+C_3\beta\right]r^*V_z^*-$$
$$-\left[C_1\frac{Br^*}{Da}r^*\left(V_z^*\right)^2+C_2MBr^*r^*\left(\frac{dV_z^*}{dr^*}\right)^2+C_3\beta\right]r^* \tag{21}$$
$$\phi(\alpha)=\frac{\alpha^2}{\eta}\left(\lambda^2+\frac{2}{\alpha}\lambda-1\right),$$
$$\psi(\alpha)=\frac{1}{\eta}\left(2-\lambda^2-\frac{4}{\alpha}\lambda\right)$$

This is a second order homogeneous differential equation with dimensionless boundary conditions, which are defined as:

$$\left.\frac{dT^*}{dr^*}\right|_{r^*=0}=0, \quad T^*\left(r^*=1\right)=0 \tag{22}$$

By double integration of Eq. (21) with the boundary conditions Eq. (22), the analytical solution of Eq. (21) is given by:

$$T^*\left(r^*\right)=t_1\left(r^*\right)^2+t_2\left[I_1(\alpha r^*)^2-I_0(\alpha r^*)^2\right]\left(r^*\right)^2+$$
$$+t_3\left[I_1(\alpha r^*)I_0(\alpha r^*)\right]r^*+t_4I_0(\alpha r^*)^2+t_5I_0(\alpha r^*)+t_6 \tag{23}$$

where t_1, t_2, t_3, t_4, t_5, and t_6 are defined as:

$$t_1=\frac{\tau\alpha}{8W}-C_1\frac{Br^*}{2Da}\frac{\alpha^2}{8W^2}-C_3\frac{\beta}{4} \tag{24}$$

$$t_2=\frac{Br^*\alpha^2}{8W^2I_0(\alpha)^2}\left(\frac{C_1}{Da}-C_2M\alpha^2\right) \tag{25}$$

$$t_3=t_2/\alpha \tag{26}$$

$$t_4=-C_2\frac{MBr^*\alpha^2}{8W^2I_0(\alpha)^2} \tag{27}$$

$$t_5=C_1\frac{Br^*}{2DaW^2I_0(\alpha)}-\frac{\tau}{2\alpha WI_0(\alpha)} \tag{28}$$

$$t_6=\frac{\tau\left(4-\alpha^2\right)}{8\alpha W}+C_3\frac{\beta}{4}+$$
$$+\frac{Br^*}{8W^2}\left[C_2M\left(\alpha^4\left(\lambda^2-1\right)+\alpha^2\left(\alpha\lambda+1\right)\right)-\right. \tag{29}$$
$$\left.-\frac{C_1}{2Da}\left(8-\alpha^2\left(3-2\lambda^2\right)+2\alpha\lambda\right)\right]$$

in which τ *and* W *are* the functions of α and are defined as:

$$\tau=\left[2+C_1\frac{\psi(\alpha)}{Da}Br^*+C_2M\phi(\alpha)Br^*+C_3\beta\right]$$
$$W=\left(\frac{\alpha}{2}-\lambda\right) \tag{30}$$

In this case, the Nusselt number Nu, based on the diameter cylinder is defined as:

$$Nu=\frac{h(2R)}{k}, \quad h=-\frac{k\left.\frac{dT}{dr}\right|_{r=R}}{\overline{T}-T_w} \tag{31}$$

$$Nu=\frac{-2}{\overline{T^*}}=-\left[c_1+c_2I_1(\alpha)+\right.$$
$$\left.+c_3I_1(\alpha)I_0(\alpha)+c_4I_0(\alpha)^2+c_5I_1(\alpha)^2\right]^{-1} \tag{32}$$

where $\overline{T^*}$ is the dimensionless average temperature and c_1, c_2, c_3, c_4 and c_5 are:

$$c_1=\frac{t_1}{4}+\frac{t_6}{2}, \quad c_2=\frac{t_5}{\alpha}, \quad c_3=\frac{t_2}{3\alpha},$$
$$c_4=\frac{t_4}{2}-\frac{t_2}{3}, \quad c_5=\frac{t_3}{2\alpha}-\frac{t_4}{2}+\frac{t_2}{3}\left(1-\frac{1}{\alpha^2}\right) \tag{33}$$

As it can be seen, the Nusselt number is a function of *Da, M*, A^*, $Br^*$and β.

Results and discussion

This section presents the investigation of the effects of variation of *Da and* A^* for the cooling process on the velocity and temperature profile, when viscous dissipation and heat generation are/ are not considered, and the Nusselt number.

As can be seen from Eq. (8), A^* changes depend on variation of the orientation angle θ and the permeability ratio parameter K^*. For $K^*<1$ and every value of θ, A^* will be less or equal to one. At zero degrees $A^*= K^*$ and with increase θ from 0 to 90 degrees A^* values were ascending and their gradient rise depended on K^* value. Meanwhile, in $\theta = 90$ for all $K^*<1$, A^* values will equal one. Therefore, $A^*<1$ describes K^* values less than 1, and also higher values of permeability amounts in z direction than in r

direction (i.e. $K_2>K_1$). In addition, whenever A^* approaches 1 (i.e. θ approaches 90 degrees), permeability in r direction to z direction enhances up to $\theta = 90$ where $K_1 = K_2$.

This interpretation can be used for $K^*>1$ where for such cases A^* is permanently above or equal to 1, so permeability in r direction is higher than in z direction, and whenever A^* approaches 1 (i.e. θ approaches 90 degree) permeability in z direction increases in relation to r direction up to $\theta = 90$, where it will be equal in both directions.

However, whenever $K^* = 1$, alterations of θ have no influence on A^* and A^* always equals 1. In this situation, permeability in both principal axes is equal.

To consider the effect of variation of Da and A^* on dimensionless normalized velocity profile and dimensionless temperature, some values should be set.

According to the inverse relation of M with porosity (ε), for ε near 1, M value will be close to 1 and for $\varepsilon<1$, the M value will be higher than 1.[1] In most literature, M value is postulated as 1. However, the research conducted by Givler and Altobelli[31] has demonstrated that the assumption of $\tilde{\mu} = \mu$ in some cases is not in good agreement with experimental results. Nevertheless, for simplification and easy comparison of these research results with other works, in this paper the M value was set as one.

In addition, some ranges were arranged for A^*, Da and Br^* to investigate the effect of variation of these parameters on dimensionless temperature and normalized velocity profiles, and Nusselt number.

Fig. 2 shows the variation of the dimensionless normalized velocity profiles $V^*(r^*)$ for different values of Darcy number Da, and directional permeability ratio parameter A^*.

According to statements about variation of A^* with K^* at the beginning of this session, $A^*<1$ indicates larger permeability in z direction relative to r direction and vice versa. Therefore, it is expected that the dimensionless normalized velocity profiles, by increasing A^* from 0.1 to 1 in constant Darcy (i.e. constant permeability in r direction) due to decrease in K_2, become wider. This trend continues when A^* increases from 1 to 10 in constant Darcy number. This trend may be observed in the lower Darcy numbers in Fig. 2.

In higher Darcy numbers, no significant variation in trend of normalized velocity profiles can be observed. But in constant Darcy numbers, by enhancing A^*, the values of $V^*(r^*)$ in the centre of the cylinder in flow direction reduce due to decrease in permeability.

It could be observed that in lower Darcy numbers and especially in higher A^*, there is uniform velocity distribution flows in most regions of the cylinder except the wall region, whereas a steep velocity gradient forms at the wall region. The high velocity gradient at the wall surface generates high rate of viscous dissipation (see Eq. (3)) which has a significant effect on dimensionless temperature profile.

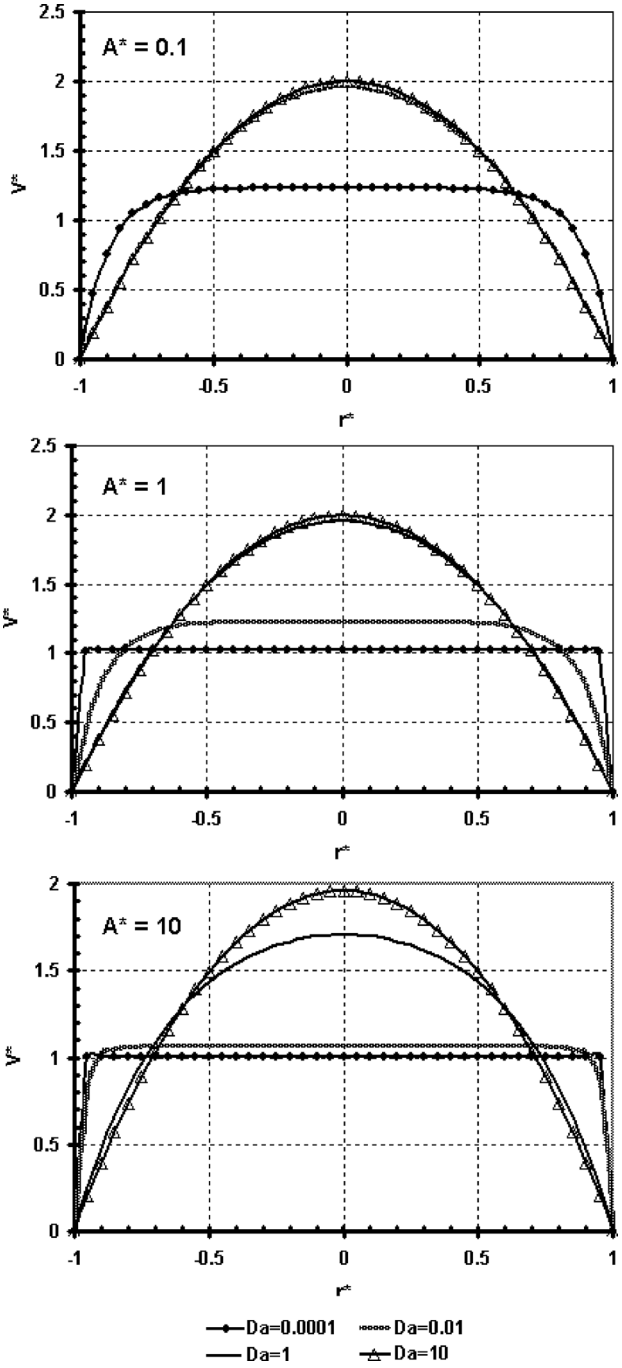

Fig. 2 – *Variations of normalized velocity profile V^* in the cylinder for different values of Da and A^**

For the cooling process $q_w < 0$, the modified Brinkman number as well as β is negative (see Eq. (19)). Also, according to cooling of the cylinder wall by q_w and consequently $T>T_w$ and the definition of dimensionless temperature in Eq. (20), it can be

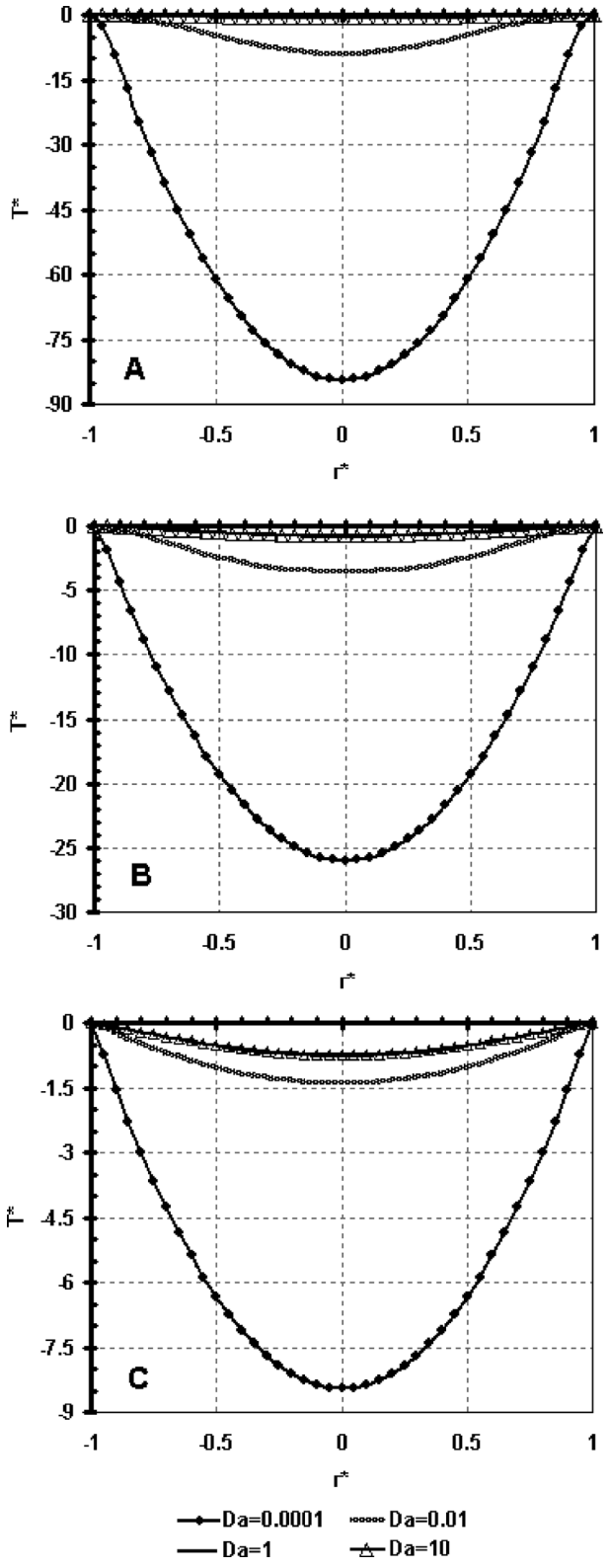

Fig. 3 – *Variations of dimensionless temperature profiles for different Darcy numbers when* $C_2 = C_3 = 0$ *(A:* $A^* = 0.1$*, B:* $A^* = 1$ *and C:* $A^* = 10$*)*

expected that the dimensionless temperature values are negative.

According to definition of β in Eq. (19) its value is set as –1. Therefore, if heat generation is considered, its value in porous media will be relative to q_w/R.

Fig. 3 illustrates the dimensionless temperature profile inside the cylinder for $C_2 = C_3 = 0$ conditions. When the internal heating effect is only considered in temperature equation, all the temperature profiles have a negative trend, as expected. These profiles in walls and the centre of cylinder have zero and maximum values, respectively (according to the boundary conditions Eq. (22)). The absolute values of dimensionless temperature profile (i.e. temperature difference between wall and fluid) decrease in the centre of cylinder with the increase in *Da* number in constant A^* values. Also, increasing A^* when *Da* number is constant, leads to reduction of absolute value of dimensionless temperature profile in the centre of the cylinder.

Small Darcy number features low permeability in the porous medium and thus induces smaller convection in a more restrictive medium. Therefore, the internal heat generation increases and in turn the fluid temperature becomes higher; hence, the temperature difference dramatically increases between cylinder wall and fluid flow.

Furthermore, for high *Da* (i.e. *Da* = 1 and 10) referring to Fig. 3, it can be perceived that the temperature distributions are identical for the cases of $A^* = 0.1$, 1, and 10, respectively. This is in agreement with the results of Hung and Tso (Figs. (2a – 2c)).[30] It can be described that, for higher *Da* numbers, which are nominated as hyper-porous medium, the internal heating effect of viscous dissipation vanishes.

When the heat generation parameter is considered in addition to internal heat in energy equation, the trend of dimensionless temperature profiles will be as shown in Fig. 4. This figure illustrates the dimensionless temperature profile inside the cylinder for $C_2 = 0$ and $C_3 = 1$ conditions. The comparison of Figs. 3 and 4, leads us to conclude that, despite adding the heat generation parameter to the energy equation, the trend of dimensionless temperature profile is not a significant change.

Fig. 5 illustrates the dimensionless temperature profile inside the cylinder for $C_2 = 1$ and $C_3 = 0$ conditions. Compared with Fig. 3 when the viscous dissipation parameter is considered in the energy equation, obvious differences are observed in the trend of $T^*(r^*)$. In higher *Da* numbers, the trend of dimensionless temperature compared to similar cases in Fig. 3 achieved negative and minimum values in walls, while there are positive and maximum values in the center of the cylinder. This trend, which is independent of A^* values, can be observed in all temperature profiles of Fig. 5. In small *Da* numbers, a different trend may be observed compared to Fig. 3, especially for $A^* = 1$ and 10. Fig. (5B) illustrates

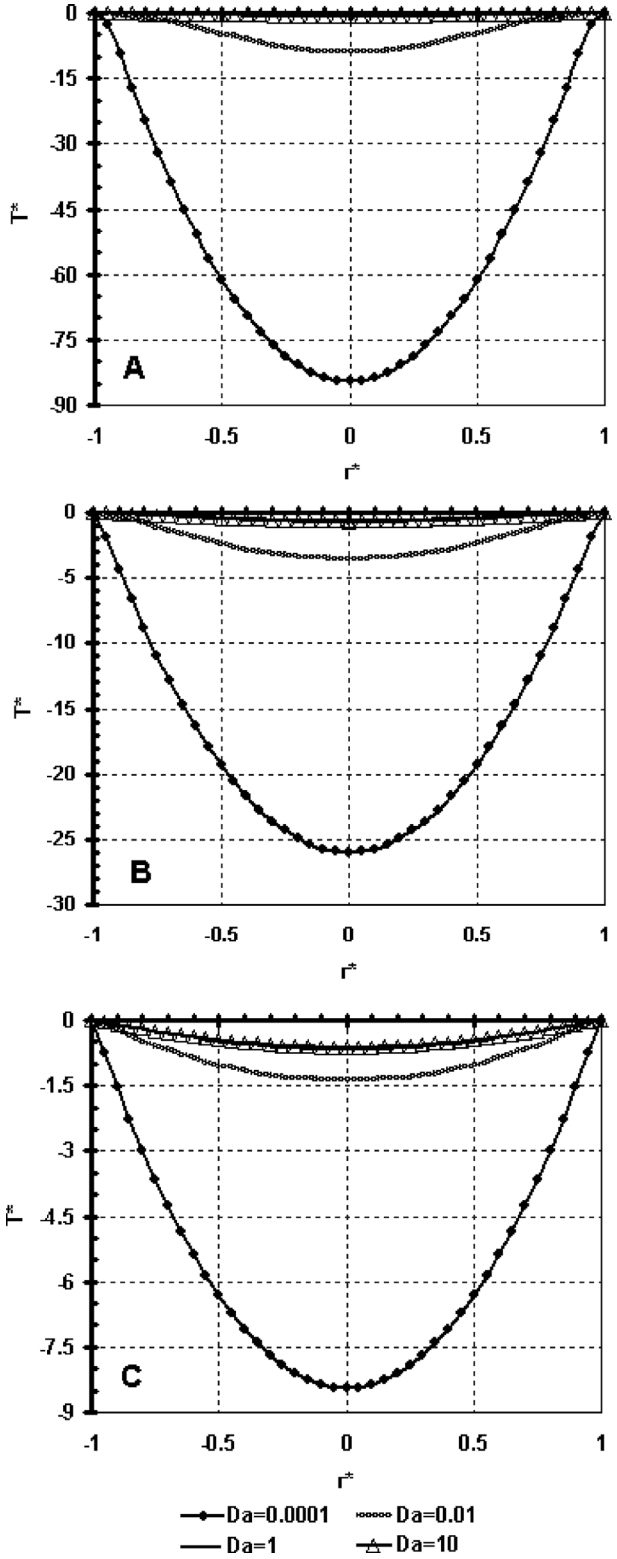

Fig. 4 – *Variations of dimensionless temperature profiles for different Darcy numbers when $C_2 = 0$ and $C_3 = 1$ (A: $A^* = 0.1$, B: $A^* = 1$ and C: $A^* = 10$)*

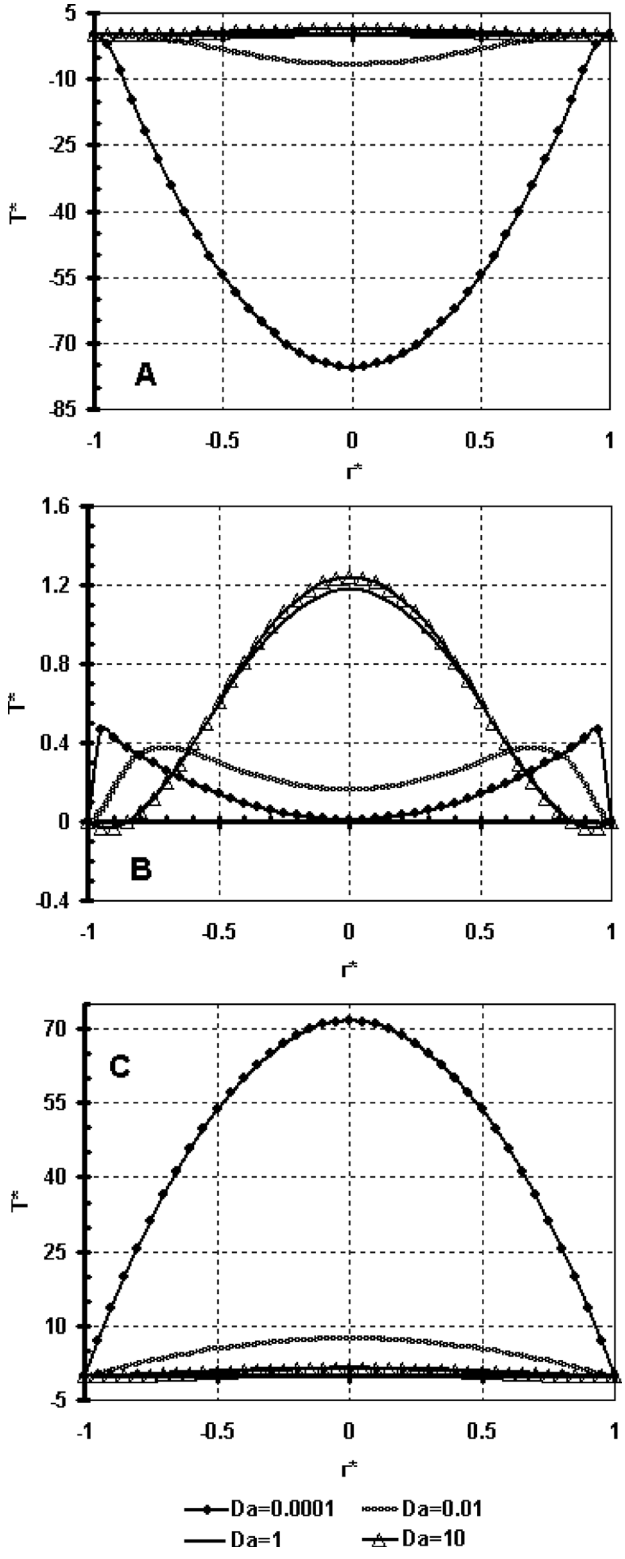

Fig. 5 – *Variations of dimensionless temperature profiles for different Darcy numbers when $C_2 = 1$ and $C_3 = 0$ (A: $A^* = 0.1$, B: $A^* = 1$ and C: $A^* = 10$)*

that, for small *Da* number, the dimensionless temperature profiles reach maximum values near the walls, while their minimum values occur in the center of the cylinder. This trend is similar to the results achieved by Hung and Tso (Fig. 9)[30] because A^*=1 means equal permeability in all directions.

This unusual trend of dimensionless temperature profile for higher and lower *Da* numbers in this figure (Figure (5-B)) may be investigated by analy-

sis of the terms of viscous dissipation treatments during cooling process. It seems that in higher *Da* numbers, due to higher frictional heating near the walls compared to internal heating in the centre of the cylinder, in spite of cooling flux to walls, the temperature of the fluid near the walls is higher than near the centre of the cylinder. In most regions inside the cylinder, this causes the dimensionless temperature profile to become positive, which indicates that the heat is transferred from walls to internal fluid. On the contrary, for lower *Da* number, the internal heating contribution in central regions is higher than frictional heating near the walls. However, this severe decrease in frictional heating has a greater influence on dimensionless temperature profiles than the increase in internal heating for small *Da* numbers. As may be observed from Fig. (5-B), fluid flows in the centre of the cylinder toward cylinder walls have higher temperature.

The interesting point of Fig. (5-B) for small Darcy numbers is the changing of the slope of the dimensionless temperature near the wall, which changed and became positive. This is the result of the offsetting effect of the increasing contribution of internal heating and decreasing contribution of frictional heating, signifying the change of direction of heat transfer at the wall for lower *Da* numbers compared to higher ones.

When A^* from 1 reaches 10 (Fig. (5-C)) for lower *Da* numbers compared to (Fig. (5-A)), the intensity of enhancement of viscous dissipation (which is mostly by frictional heating) in cylinder wall is high, and on other side, internal heating in centre regions near the walls is lower. Therefore, this causes temperature of the near-wall fluid to become higher than the central regions, and heat transfer, in spite of cooling flux, occurs from wall to fluid. Thus, contrary to $A^* = 0.1$, the temperature profiles at $A^* = 10$ and lower *Da* number take positive values. This change in direction of heat transfer by enhancement of *Da* number and A^* represents changes in Nusselt number (*Nu*) sign which will be discussed later.

Fig. (6) illustrates the dimensionless temperature profile inside the cylinder for $C_2 = 1$ and $C_3 = 1$ conditions. When the heat generation parameter is included in the energy equation in addition to frictional heating parameter, the dimensionless temperature profile undergoes no appreciable changes compared to that in Fig. (5). This indicates that the heat generation parameter, shown by β, in all cases has very little effect on the temperature profile.

In order to validate the accuracy of the dimensionless temperature gradient trend by r^* for different Darcy numbers, it was compared with other works, such as reference.[30] In that research, the permeability was considered constant and the model

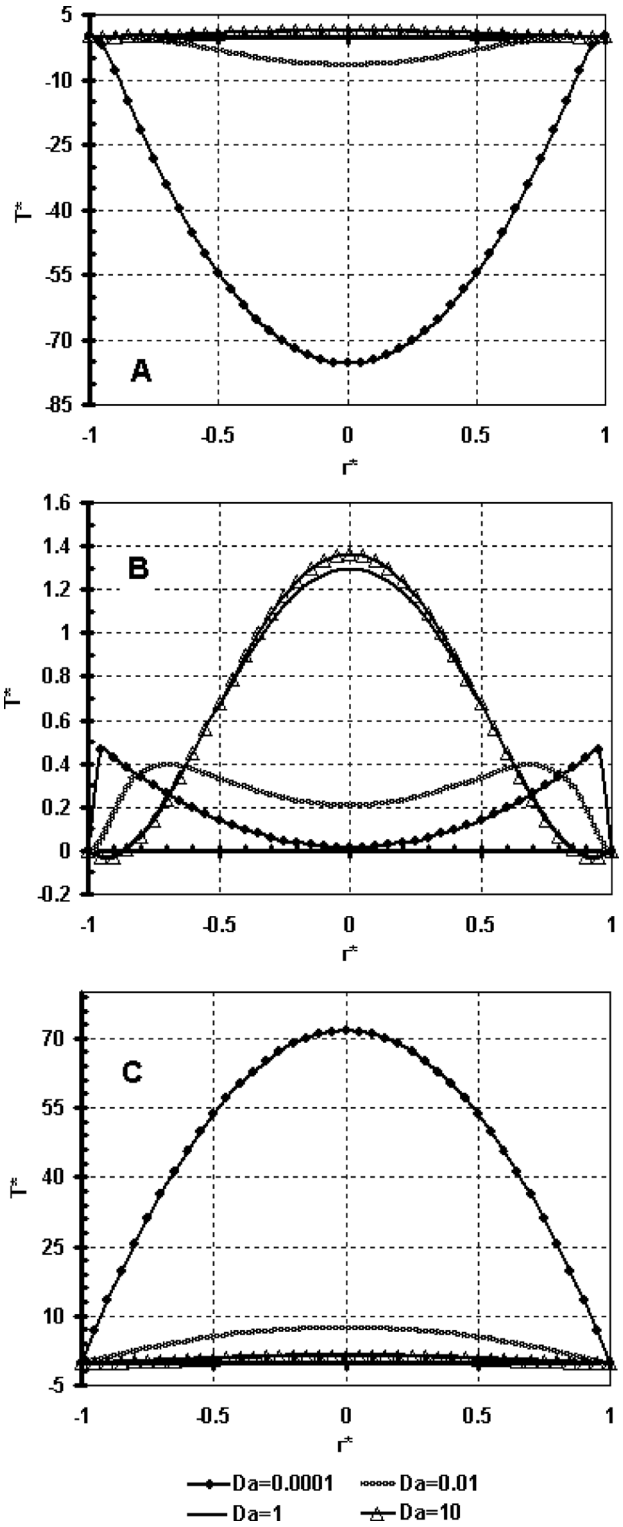

Fig. 6 – *Variations of dimensionless temperature profiles for different Darcy numbers when $C_2 = C_3 = 1$ (A: $A^* = 0.1$, B: $A^* = 1$ and C: $A^* = 10$)*

did not mention the heat generation parameter. Therefore, in our model the amounts of A^* and C_3 were equal to 1 and 0, respectively. Fig. (7) illustrates the trend of dimensionless temperature gradient for different Darcy numbers, which are the same in both models. The difference in numerical amount

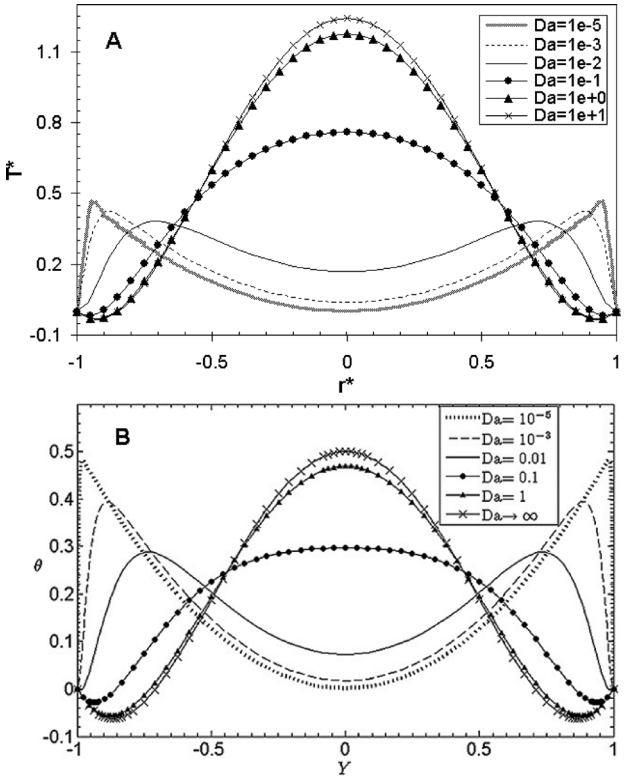

Fig. 7 – *Variation of dimensionless temperature in the width of channels when* $Br^* = -1$. *A: Current study and B: Study.*[30]

of models is because of their geometric structure. (It is worth noting that in Fig. (7-A), the $Da = 10$ could be approximately considered $Da \to \infty$)

Fig. (8) shows Nusselt number variations based on A^* for four values of Da and different changes of C_2 and C_3 for cooling process (i.e. $Br^* = -1$).

When the frictional heating term is not considered, as observed previously in dimensionless temperature profiles, the presence or absence of heat generation does not significantly change the trend of Nusselt number with A^*. Figs. (8-A) and (8-C) show this result clearly.

For lower Da numbers (Figs. (8-A) and (8-C)), an increase in A^* leads to enhanced Nusselt number, which for very small Da numbers (i.e. $Da = 10^{-4}$) is slower, while for higher Da numbers (i.e. $Da = 10^{-2}$) this occurs more abruptly. As illustrated in these figures, this increase in Da number higher than 1, is oriented toward a specific number, so that for very large Da numbers (i.e. $Da = 10$), the Nusselt number is constant despite A^* changes. This constant value for the case where heat generation parameter is ignored, equals 5.981 (Fig. (8-A)), and equals 6.813 (Fig. (8-C)). Such trend of Nusselt number may be observed in Hung and Tso work (Fig. (4-b)),[32] which for a rectangular channel in a cooling process, the Nusselt number equalled 4.118 when heat

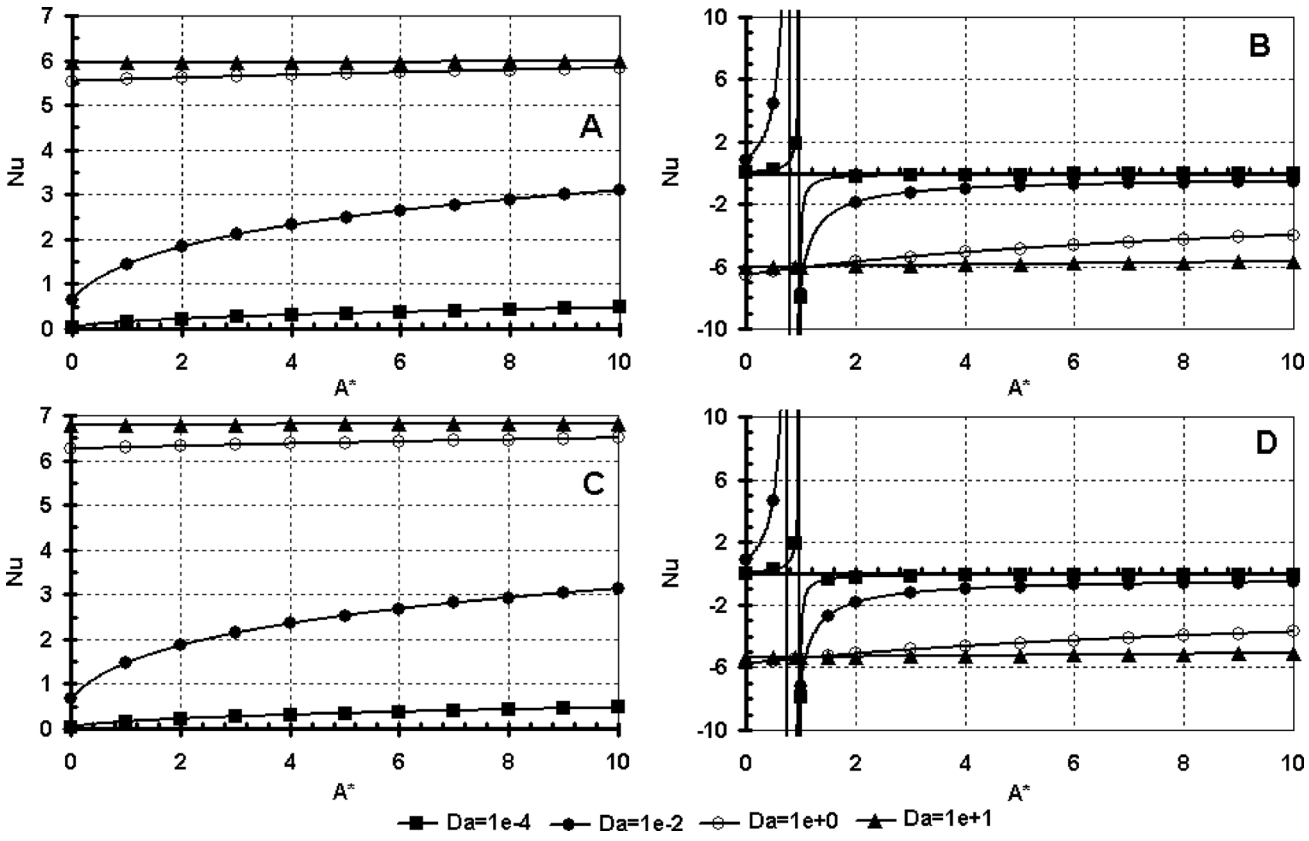

Fig. 8 – *Variations of Nusselt number with* A^* *for different Darcy numbers (A:* $C_2 = C_3 = 0$, *B:* $C_2 = 1$, $C_3 = 0$, *C:* $C_2 = 0$, $C_3 = 1$ *and D:* $C_2 = C_3 = 1$*)*

generation and frictional heating terms were ignored.

When frictional heating term in the energy equation is considered, as expected, the Nusselt number sign will change. This change will happen in lower *Da* numbers. For $Da = 10^{-4}$ in $A^* = 0.98$ and for $Da = 10^{-2}$ it occurs in $A^* = 0.783$ and 0.7675, respectively (see Figs. (8-B) and (8-D)).

This A^* where direction of heat transfer changes from wall to fluid or from fluid to wall is called critical directional permeability ratio parameter (A_C^*).[12] For $A_C^* < 0.98$ when $C_2 = C_3 = 1$ and $Da = 10^{-4}$, dimensionless temperature values become negative, which represents lower temperature of the wall compared to fluid, and direction of heat transfer is from fluid to walls (Fig. (6-A) for $A^* = 0.1$). However, for $A_C^* > 0.98$, dimensionless temperature values are positive, indicating a change in the direction of heat transfer. Whereas, in this case heat transfers from walls to fluid inside the channel (Figs. (6-B) and (6-C) for $A^* = 1$, and 10).

By comparing Figs. (8-B) and (8-D) and Figs. (8-A) and (8-C) in high Darcy numbers, the Nusselt number sign changes. The reason for this sign change may be described by comparing dimensionless temperature profiles in Figs. (5) and (6) with Figs. (3) and (4), because when the frictional heating term is ignored, the dimensional temperature profiles take negative values, while when considering this parameter they take positive values. This change in dimensional temperature profile trend is the reason for the sign change of Nusselt number.

The validity of the resulting model to describe the variation of Nusselt number with A^* was verified by comparison with other models, such as the work in reference.[12] In their investigation, they also applied the rectangular channel without heat generation parameter. Therefore, in the resulting model, the situation where $C_3 = 0$ was selected. As Fig. (9) shows, the trend of variation of *Nu* with A^* is the same in both models. The *Nu* changes for both models occurred in small *Da* numbers. For example, when $Da = 0.01$, the *Nu* changes for the cylinder and rectangular model in $A^*_c = 0.783$ and 0.895, respectively. The difference is because of various models and different Nusselt number definition.

Figs. (10), (11) and (12) illustrate Nusselt number variation with different *Da* and Br^* for A^* values of 0.1, 1 and 10 respectively. When $A^* = 0.1$ and frictional heating is ignored (Figs. (10-A) and (10-C)), all Nusselt numbers are positive and their trend ascends with the increase in *Da* number for all Br^* values. This trend is predictable according to the similarity in dimensional temperature profiles for these two cases at $A^* = 0.1$ (Figs. (3-A) and (4-A)). For cooling process, as shown in Figs. (10-A) and (10-C), the Nusselt number asymptotes to

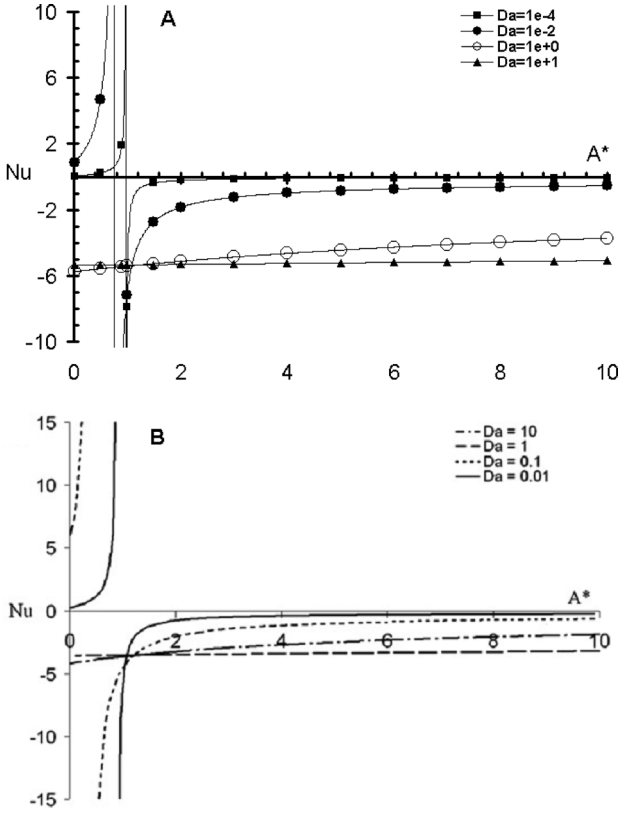

Fig. 9 – *Variation of Nusselt number with A^* when $Br^* = -1$. A: Cylinder model, and B: Rectangular model*[12]

$Nu_\infty = 5.999$ for $C_3 = 0$ and $Nu_\infty = 6.856$ for $C_3 = 1$ at higher *Da* number. Also, the Nusselt number approaches Nu_∞ faster for smaller Br^* in terms of absolute value.

However, when the frictional heating term is considered, the Nusselt number trend changes completely. As may be seen in Fig. (10-B), for every Br^* value except –0.1, the Nusselt number sign changed (for $Br^* = -10$ and –20 in $Da = 0.0375$ and for $Br^* = -1$ in $Da = 0.0755$ in Fig. (10-C), and for $Br^* = -10$ and –20 in $Da = 0.0375$ and for $Br^* = -1$ in $Da = 0.068$ in Fig. (10-D)). The reason for this trend lays in the velocity and temperature profile treatment in especially low *Da* numbers. As for $A^* = 0.1$ in Fig. (2), there was a steep slope for the dimensionless normalized velocity profile near the walls. By considering the frictional heating term and Eq. (3), this steep slope may be seen in the dimensionless temperature profile, leading the heat transfer direction to change from centre to walls to walls to centre. Therefore, the sign of Nusselt number changes in smaller *Da* numbers for $Br^* = -1$, –10 and –20. For smaller modified Brinkman numbers (i.e. $Br^* = -0.1$) in terms of absolute value, because of the Br^* role as a measure of importance of the viscous dissipation term, due to decreasing its importance (which is the reason for its fractional

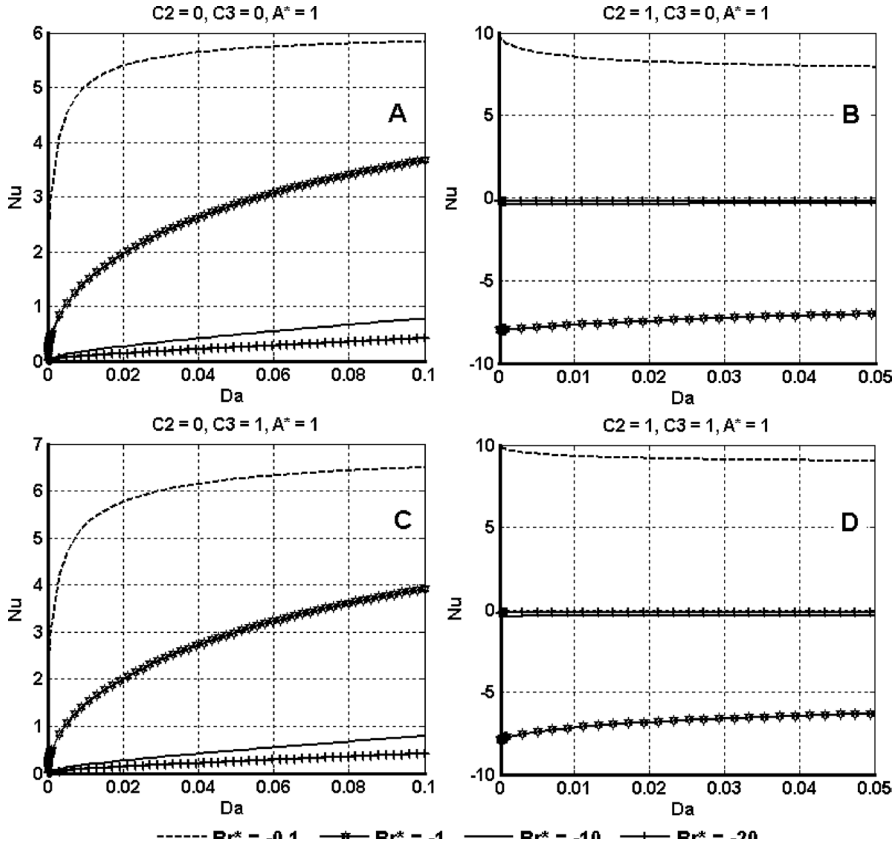

Fig. 10 – *Variations of Nusselt number with Da for different Br* when A* = 0.1 and different C_2 and C_3*

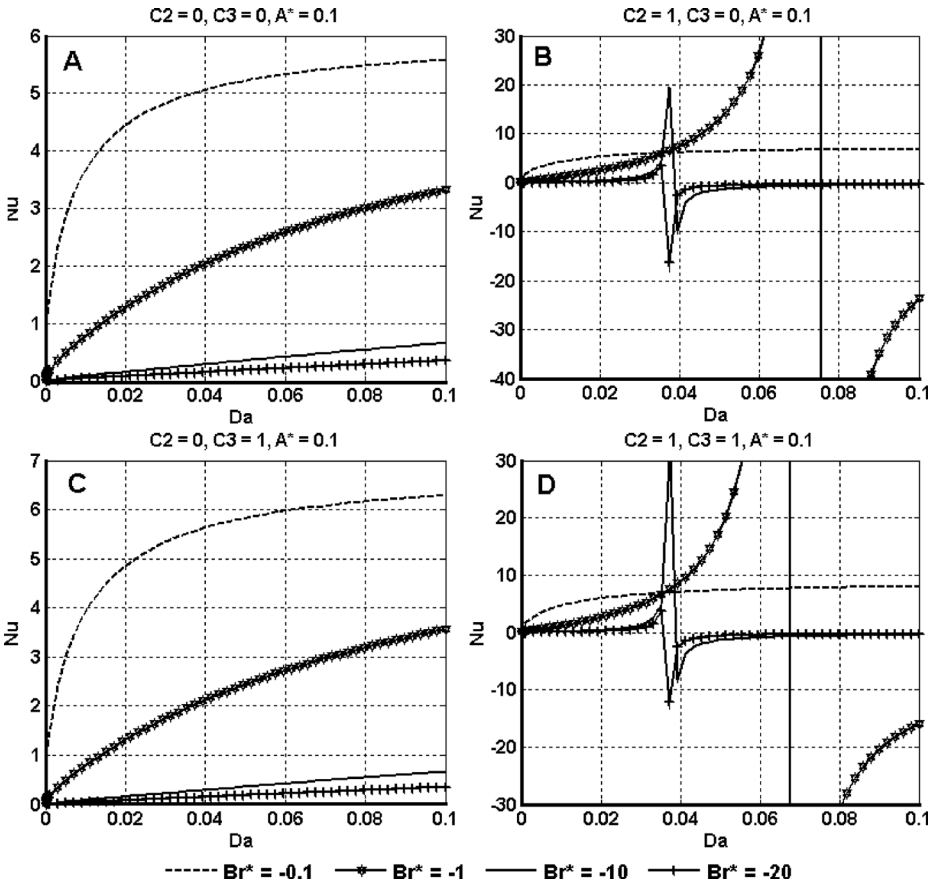

Fig. 11 – *Variations of Nusselt number with Da for different Br* when A* = 1 and different C_2 and C_3*

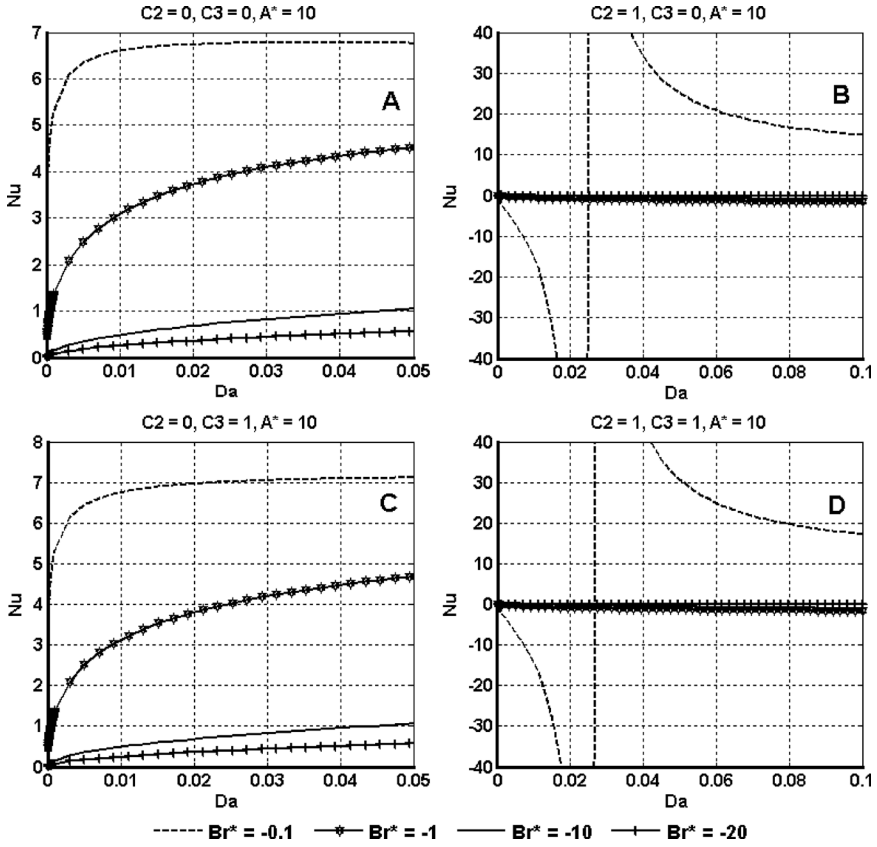

Fig. 12 – *Variations of Nusselt number with Da for different Br^* when $A^* = 10$ and different C_2 and C_3*

heating term reduction), no sign change of Nusselt number can be confirmed.

When A^*=1, the trend of Nusselt number by increasing the *Da* number when $C_2 = 0$ (Figs. (11-A) and (11-C)) is almost similar to $A^* = 0.1$ (this similarity was expected by comparison of dimensionless temperature profiles for these cases). However, for $C_2 = 1$ (Fig. (11-B)), significant changes occur in Nusselt number trend by increasing the *Da* number, except for $Br^* = -0.1$. Other modified Brinkman numbers have an upward trend, while for $Br^* = -0.1$ this trend is descending. Also, for all Br^* when *Da* number tends toward infinity, the Nusselt number tends toward a constant number ($Nu_\infty = 8.88$ for $Br^* = -0.1$, $Nu_\infty = -5.33$ for $Br^* = -1$, $Nu_\infty = -0.3137$ for $Br^* = -10$ and $Nu_\infty = -0.1534$ for $Br^* = -20$).

In addition, when modified Brinkman number reaches from –0.1 to –1, the Nusselt number sign for all *Da* numbers changes, which indicates that the direction of heat transfer changes from wall to fluid or vice versa.

When $A^* = 10$, the Nusselt number trend ascends with the increase in *Da* number for all of Br^*, in the absence of frictional heating term in the energy equation (i.e. $C_2 = 0$) (Figs. (12-A) and (12-C)). In addition, when $C_2 = 0$, the Nusselt number tends toward a constant number with the increase in *Da* number, for all Br^*. ($Nu_\infty = 6$ for $C_3 = 0$ (Fig. (12-A)) and $Nu_\infty = 6.858$ for $C_3 = 1$ (Fig. (12-C)).

When $C_2 = 1$, the sign of Nusselt number for all Br^* except –0.1 is negative and descends with increase in *Da* number, while for $Br^* = -0.1$ in $Da = 0.025$ (Fig. (12-B)) and in $Da = 0.0267$ (Fig. (12-D)) a sign change of Nusselt number occurred. This trend is almost in contrariwise trend of *Nu* number depicted in Fig. (10), and it is acceptable when dimensionless temperature profiles for $A^* = 0.1$ and 10 for small *Da* numbers, and when $C_2 = 1$ are compared. As may be seen in Figs. (6-A) and (6-C) for smaller *Da* numbers the dimensionless temperature profile is negative when $A^* = 0.1$, and positive when $A^* = 10$.

The equation below was considered for better investigation of the effect of the presence or absence of frictional heating term in Nusselt number:[30]

$$\delta = \frac{Nu_0 - Nu}{Nu} \tag{34}$$

Nu_0 is the Nusselt number when $C_2 = 0$ (in case when frictional heating term is ignored). In fact, δ values represent the deviation of Nusselt number in the case when frictional heating term is not considered.

Fig. (13) illustrates δ charts vs. *Da* numbers for different A^* and Br^* for two cases of the pres-

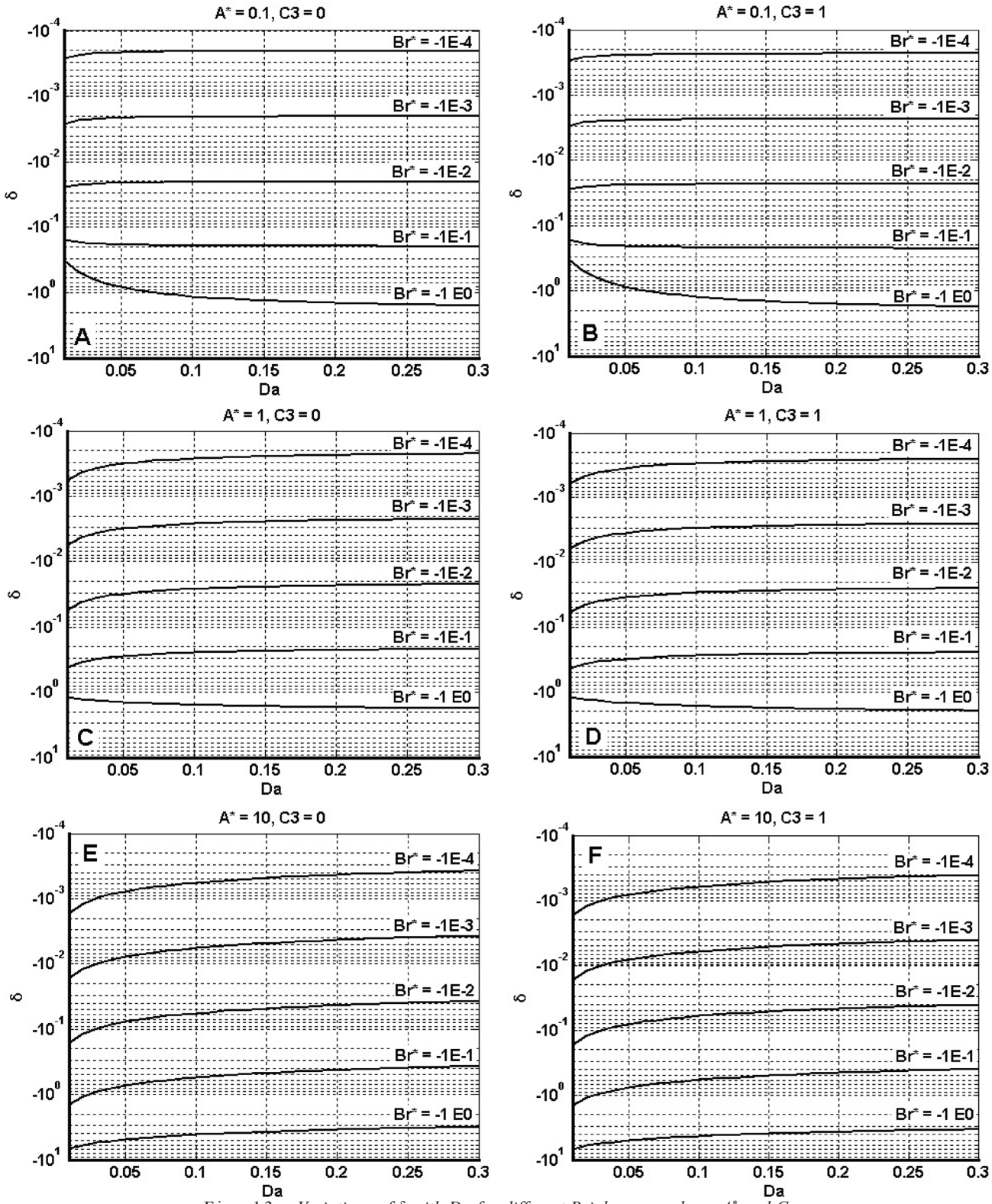

Fig. 13 – *Variations of δ with Da for different Brinkman numbers, A^* and C_3*

ence and absence of heat generation term. The negative values of δ are due to cooling process when $Br^*<0$. This figure indicates that, if fractional heating term is not considered, the Nusselt number for the cooling process is estimated to be lower.

As these figures depict, δ variations for all Br^* in small *Da* numbers are more significant. While for higher *Da* numbers, it is negligible. This trend of δ for this range of *Da* numbers, especially for $A^*= 1$ is in agreement with the results of Hung and Tso research for rectangular channel (Fig. (10)).[30]

Trend of absolute values of δ by increasing *Da* numbers when $A^*>1$ for all Br^* is descending, while for $A^* = 1$ the trend of absolute values of δ by increasing *Da* numbers for $Br^* = -1$ is ascending, and for other Br^* values is descending. Also, when $A^*<1$ this trend is ascending for $Br^* = -0.1$ and -1, and for other Br^* values is descending.

Furthermore, for all very small absolute values of Br^* ($Br^* = -0.001, -0.0001$), the absolute values of δ by increasing *Da* numbers, gradually tend toward zero. This confirms that for these Br^* values there is no significant difference between *Nu* and Nu_0 while this difference is significant for higher absolute values of Br^*. In addition, the presence or absence of heat generation has no impressive effect on trends of δ versus *Da* by different values of A^* and Br^*.

The results of variations of δ by *Da* numbers especially for small Darcy numbers were validated by the results of reference,[30] which are depicted in Fig. (14). As mentioned before, due to the non-existence of the heat generation parameter and constant permeability in the model used in the reference,[30] the amount of C_3 and A^* were chosen as zero and 1, respectively. This model was suggested for a rectangular channel, but the trend of variations of δ with *Da,* especially for small *Da* numbers, is in accordance with the present model. Nevertheless, there are some differences between these two models, which originate from their different physical characteristics.

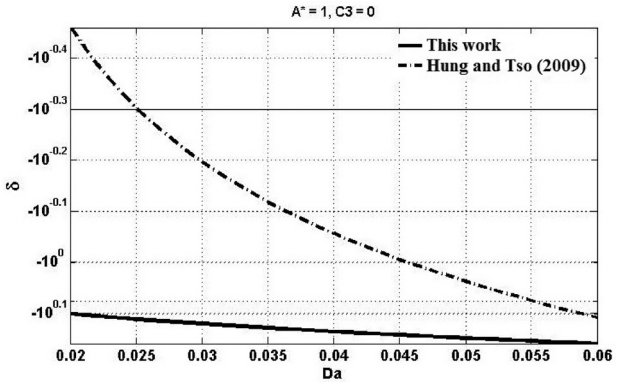

Fig. 14 – *Comparison of results of variations of δ with Da when $Br^* = -1$ with*[30]

Fig. (15) shows the variations of δ with A^* for different Darcy and modified Brinkman numbers. As mentioned in Fig. (13), for all values of Br^*, variations of δ in smaller Darcy numbers were more significant, which is also observable in Fig. (15). The considerable point about Fig. (15) is the coalescence of variations of δ for $Br^* = -0.1$ and -1 at specific values of A^*. This phenomenon can be described from Fig. (13). In these charts, by increasing *Da,* the graph related to $A^* = 0.1$ and 1 for $Br^* = -1$ is descending, which decreases by enhancement of A^*. Meanwhile, it will be ascending when $A^* = 10$. Also, for $Br^* = -0.1$, this special A^* value is between 0.1 and 1. This demonstrated that when A^* values are between 1 and 10 for $Br^* = -1$, and when A^* values are between 0.1 and 1 for $Br^* = -0.1$, variations of δ with *Da* are like a straight line. As may be observed from Fig. (15), the value of this A^* for $Br^* = -1$ and $C_3 = 0$ is exactly equal to 2, and when $C_3 = 1$, it is around 2.3 (see Figs. (15-G) and (15-H), respectively), while for $Br^* = -0.1$ when $C_3 = 0$ (Fig.(15-E)) and $C_3 = 1$ (Fig. (15-F)) is equal to 0.2 and 0.25, respectively.

Furthermore, as the Br^* values tend toward zero, the special A^* values (A_V^*) also tend toward zero. However, the absence of δ changes with *Da* for $Br^*>-1$ (these figures are not included in this paper), in terms of absolute magnitude, for larger A^* values, confirmed that these special A^* values are directly related to how Br^* values change. This relation can be considered for $C_3 = 0$ with good accuracy as follows:

$$A_V^* = -2\ Br^* \tag{35}$$

Where A_V^* is the special value of A^*. These special A^* values indicate that Nusselt number will not change with *Da* variations by taking or not taking the fractional heating parameter in energy equation (Eq. (3)) and will be a constant value.

Conclusion

In this work, the effects of anisotropic flow permeability on convection inducted in a cylinder with internal heat generation for constant cooling heat flux boundary conditions have been examined in detail for fully developed flow. This kind of problem may occur in a fixed bed catalytic reactor with an exothermic reaction.

To evaluate the effect of the presence or absence of fractional heating and heat generation, as well as variations of Darcy numbers, Br^* and A^* on temperature profiles, Nusselt number and velocity profiles, a wide range of values for these parameters were considered.

For normalized velocity profiles, it was considered that by increasing A^*, high velocity gradient appeared in the region close to the cylinder wall. This is the reason for the high heat generation resulting from viscous dissipation, which occurs at regions close to the wall, especially for smaller values of *Da* and large values of A^*.

The variation of *Nu* with A^* as well as *Da* for different values of Br^* when fractional heating and heat generation parameters are/are not considered in

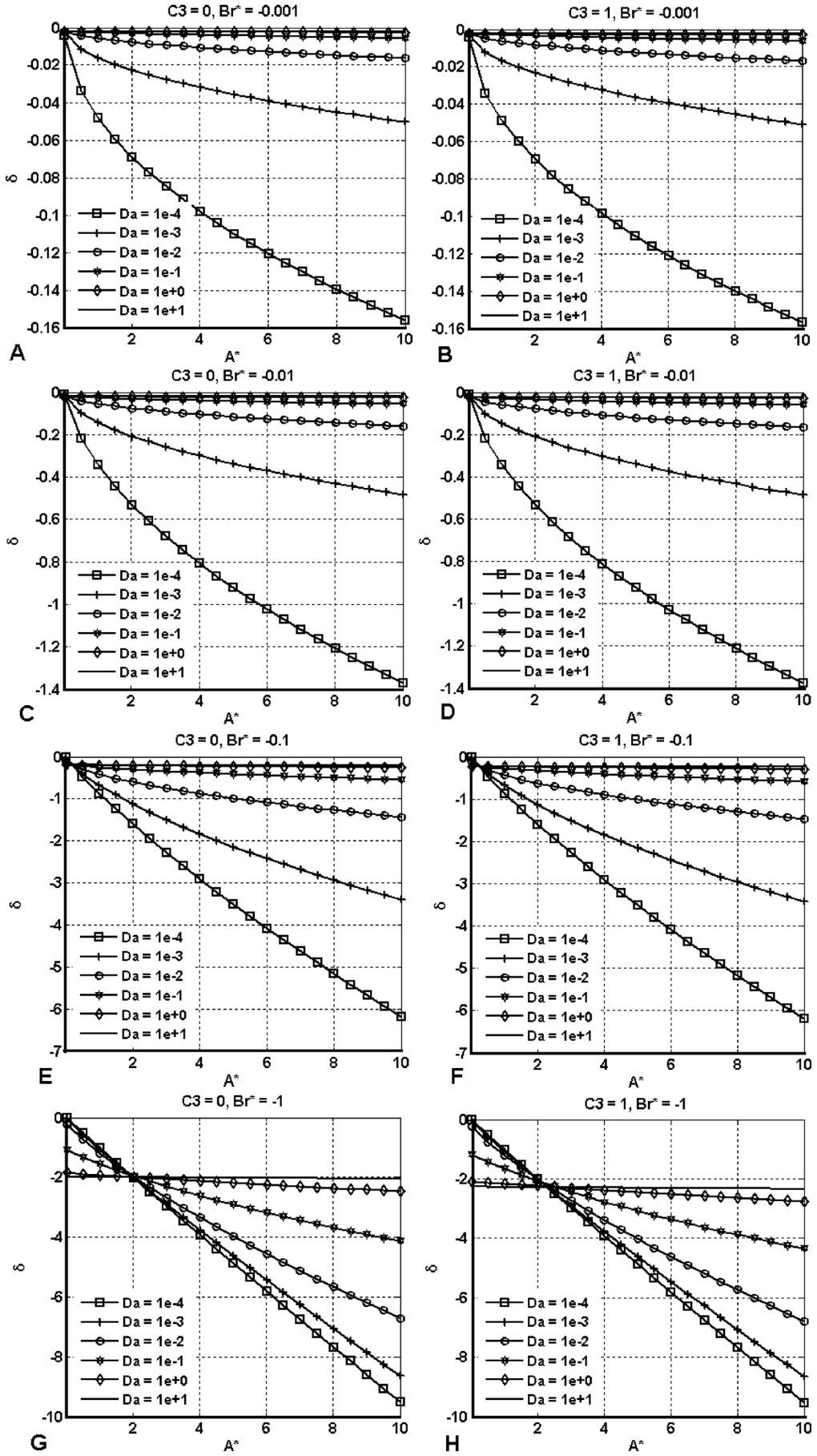

Fig. 15 – *Variations of δ with Da when Br *= –1*

the energy equation, shows that there is singularity in *Nu* at which the sign of heat transfer changes. These A^* values in which the direction of heat transfer were changed are designated by A_C^*.

To investigate the effect of the presence or absence of the frictional heating term on Nusselt number, a parameter δ was defined, which described the deviation of *Nu* for the case when the frictional heating term is not considered. By studying the variations of this parameter with Darcy number for different A^* and Br^* values, it was found that in very small Darcy numbers, variations of δ for all A^* values were significant, but when Darcy number increased, the rate of these variations decreased. For specific values of A^* which is designated as A_V^*, variations of δ with *Da* were zero. These special values of A^* are equal to the double amount of Br^* values, especially when heat generation parameter is not considered in the energy equation.

ACKNOWLEDGMENT

The authors would like to acknowledge Ahar Branch of Islamic Azad University (Iran) for financial support of this research, which is based on a research project contract.

Nomenclature

A^* – directional permeability ratio parameter
A_C^* – critical directional permeability ratio parameter
A_V^* – special directional permeability ratio parameter
Br^* – modified Brinkman number
c_1, c_2, c_3, c_4, c_5 – coefficients in Eq. (32)
C_1, C_2, C_3 – constant coefficients [0 and 1] in Eq. (3)
C_p – specific heat at constant pressure, J kg^{-1} K^{-1}
Da – Darcy number
K_1, K_2 – flow permeability along the principle axes (m^2)
K^* – permeability ratio parameter (K_1/K_2)
$\overline{\overline{K}}$ – symmetrical second order permeability tensor
M – dimensionless viscosity parameter ($\tilde{\mu}\ /\mu$)
Nu – Nusselt number
Nu_∞ – Nusselt number in higher *Da*
P – pressure (Pa)
q_w – constant wall heat flux, W m^{-2}
q''' – uniform heat generation, W m^{-3}
r – coordinate normal to the surfaces of the channel
R – diameter of cylinder, m
r^* – dimensionless coordinate in *r* direction
t_1, t_2, t_3, t_4, t_5, t_6 – coefficients in Eq. (23)
T – volume-averaged equilibrium temperature for both solid and fluid, K
T_w – wall temperature, K
T^* – dimensionless temperature
$\overline{T}$ – average temperature, K
$\overline{T^*}$ – dimensionless average temperature
$\vec{V}$ – superficial flow velocity victor
V_r – velocity in r-direction, m s^{-1}
V^* – dimensionless normalized velocity
V_z – velocity in z-direction, m s^{-1}
$\bar{V}_z$ – average velocity, m s^{-1}
W – coefficient in Eq. (30)
z – coordinate along the axis of the channel

Greek letters

α – dimensionless anisotropy factor
β – dimensionless term of heat flux and heat generation, Eq. (19)
γ – negative of the applied pressure gradient, Pa s kg^{-1}
δ – relative deviation of Nusselt numbers
ε – porosity
η – dimensionless parameter, Eq. (19)
θ – orientation angle, $0 \le \theta \le 90°$
λ – dimensionless parameter, Eq. (19)
μ – viscosity of the fluid, kg m^{-1} s^{-1}
$\tilde{\mu}$ – effective viscosity, kg m^{-1} s^{-1}
ρ – fluid density, kg m^{-3}
τ – coefficient in Eq. (30)

References

1. *Nield, D. A., Bejan, A*. Convection in Porous Media, Springer, New York, 2006.
2. *Journeau, C., Haquet, J.-F*., Nuc. Eng. Des. **239** (2009) 389. http://dx.doi.org/10.1016/j.nucengdes.2008.10.020
3. *Ennis-King, J., Preston, I., Paterson, L.,* Phys. Fluids (1994-present) **17** (2005).
4. *Neale, G.,* AIChE **23** (1977) 56. http://dx.doi.org/10.1002/aic.690230110
5. *Yovogan, J., Degan, G.,* J. Eng. Math. **81** (2013) 127. http://dx.doi.org/10.1007/s10665–012–9605–6
6. *Malashetty, M. S., Shivakumara, I. S., Kulkarni, S.,* Transp. Porous Med. **60** (2005) 199. http://dx.doi.org/10.1007/s11242–004–5130-z
7. *Mariani, N. J., Keegan S. D.,, Martínez, O. M., Barreto, G. F.,* Chem. Eng. J. **198–199** (2012) 397. http://dx.doi.org/10.1016/j.cej.2012.05.101
8. *Roper, C. S., Fink, K. D., Lee, S. T., Kolodziejska, J. A.,* Jacobsen, *A. J.,* AIChE **59** (2013) 622. http://dx.doi.org/10.1002/aic.13821
9. *Bhadauria, B. S., Kumar, A. Kumar, J. Sacheti, N., Chandran, P.,* Transp. Porous Med. **90** (2011) 687. http://dx.doi.org/10.1007/s11242–011–9811–0
10. *Dhanasekaran, M. R., Das, S. K., Venkateshan, S. P.,* J. Heat Tran. **124** (2002) 203. http://dx.doi.org/10.1115/1.1418700
11. *Degan, G., Vasseur, P.,* Numer. Hat TR A-Appl. **30** (1996) 397. http://dx.doi.org/10.1080/10407789608913847
12. *Mobedi, M., Cekmer, O., Pop, I.,* Int. J. Therm. Sci. **49** (2010) 1984. http://dx.doi.org/10.1016/j.ijthermalsci.2010.06.002

13. *Vasantha, R., Nath, G.,* Int. Commun. Heat Mass **14** (1987) 639. http://dx.doi.org/10.1016/0735–1933(87)90043–1
14. *Degan, G., Zohoun, S., Vasseur, P.,* Int J. Heat Mass **45** (2002) 3181. http://dx.doi.org/10.1016/S0017–9310(02)00032–7
15. *Al-Hadhrami, A. K., Elliott, L., Ingham, D. B.,* Transp. Porous Med. **49** (2002) 265. http://dx.doi.org/10.1023/A:1016290505000
16. *Degan, G., Vasseur, P.,* Int. J. Eng. Sci. **40** (2002) 193. http://dx.doi.org/10.1016/S0020–7225(01)00012-X
17. *Cekmer, O., Mobedi, M., Ozerdem, B., Pop, I.,* Transport Porous Med. **90** (2011) 791. http://dx.doi.org/10.1007/s11242–011–9816–8
18. *Castinel, G., Combarnous, C.,* Comptes Rendus de l'Académie des Sciences **278** (1974) 701.
19. *Epherre, J. P.*, Rev. Gen. Therm. **168** (1975) 949.
20. *Kvernvold, P. O., Tyvand, P. A.*, J. Fluid Mech. **90** (1979) 609. http://dx.doi.org/10.1017/S0022112079002445
21. *Tyvand, P. A., Storesletten, L.,* J. Fluid Mech. **226** (1991) 371. http://dx.doi.org/10.1017/S0022112091002422
22. *Malashetty, M. S., Begum, I.,* Transp Porous Med. **88** (2011) 315. http://dx.doi.org/10.1007/s11242–011–9741-x
23. *Malashetty, M. S., Kollur, P.,* Transp Porous Med. **86** (2011) 435. http://dx.doi.org/10.1007/s11242–010–9630–8
24. *Kuznetsov, A. V., Nield, D. A.,* J. Porous Med. **6** (2003) 7. http://dx.doi.org/10.1615/JPorMedia.v6.i1.30
25. *Poulikakos, D., Renken, K.,* Trans. ASME **109** (1987) 880. http://dx.doi.org/10.1115/1.3248198
26. *Hooman, K., Ranjbar-Kani, A. A.,* Int. Comm. Heat Mass Transfer **30** (2003) 1015. http://dx.doi.org/10.1016/S0735–1933(03)00160-X
27. *Minkowycz, W. J., Cheng, P.,* Int J Heat Mass **19** (1976) 805. http://dx.doi.org/10.1016/0017–9310(76)90135–6
28. *Degan, G., Gibigaye, M., Akowanou, C., Awanou, N. C.,* J Eng Math. **62** (2008) 277. http://dx.doi.org/10.1007/s10665–007–9211–1
29. *Ingham, D. B., Pop, I., Cheng, P.,* Transp. Porous Med. **5** (1990) 381. http://dx.doi.org/10.1007/BF01141992
30. *Hung, Y.-M., Tso, C. P.,* Int Commun Heat Mass **36** (2009) 597. http://dx.doi.org/10.1016/j.icheatmasstransfer.2009.03.008
31. *Givler, R., Altobelli, S.,* J. Fluid Mech. **258** (1994) 355. http://dx.doi.org/10.1017/S0022112094003368
32. *Hung, Y. M., Tso, C. P.,* Transp Porous Med. **75** (2008) 319. http://dx.doi.org/10.1007/s11242–008–9226–8